University of Pennsylvania
ScholarlyCommons

Department of Physics Papers

Department of Physics

8-7-2007

Branching, Capping, and Severing in Dynamic Actin Structures

Anjay Gopinathan
University of California

Kun-Chun Lee
University of Pennsylvania

Jennifer Schwarz
Syracuse University

Andrea J. Liu
University of Pennsylvania, ajliu@physics.upenn.edu

Follow this and additional works at: http://repository.upenn.edu/physics_papers

Part of the Physics Commons

Branching, Capping, and Severing in Dynamic Actin Structures

Abstract

Branched actin networks at the leading edge of a crawling cell evolve via protein-regulated processes such as polymerization, depolymerization, capping, branching, and severing. A formulation of these processes is presented and analyzed to study steady-state network morphology. In bulk, we identify several scaling regimes in severing and branching protein concentrations and find that the coupling between severing and branching is optimally exploited for conditions *in vivo*. Near the leading edge, we find qualitative agreement with the *in vivo* morphology.

Disciplines

Physical Sciences and Mathematics | Physics

P H Y S I C A L   R E V I E W   L E T T E R S

Branching, Capping, and Severing in Dynamic Actin Structures

Ajay Gopinathan,[1] Kun-Chun Lee,[2] J. M. Schwarz,[3] and Andrea J. Liu[2]

[1]*School of Natural Sciences, University of California, Merced, California 95344, USA*
[2]*Department of Physics and Astronomy, University of Pennsylvania, Philadelphia, Pennsylvania 19104, USA*
[3]*Department of Physics, Syracuse University, Syracuse, New York 13244, USA*

Branched actin networks at the leading edge of a crawling cell evolve via protein-regulated processes such as polymerization, depolymerization, capping, branching, and severing. A formulation of these processes is presented and analyzed to study steady-state network morphology. In bulk, we identify several scaling regimes in severing and branching protein concentrations and find that the coupling between severing and branching is optimally exploited for conditions *in vivo*. Near the leading edge, we find qualitative agreement with the *in vivo* morphology.

When a cell crawls, it must reorganize the cytoplasmic network of biopolymers that controls its shape. The shape and motility of the leading edge (the lamellipodium) of a crawling cell are determined primarily by a dynamic network of actin filaments (*F*-actin) [1]. These filaments are living polymers made up of monomeric *G*-actin, and have a definite polarity such that monomers tend to be added to the plus (or "barbed") end, and tend to fall off at the minus (or "pointed") end. A host of regulatory proteins concentrate plus ends at the leading edge by controlling the morphology of the actin filament network [2]: capping proteins bind to the plus end of filaments, preventing further growth, severing proteins, such as cofilin, bind to filaments and break them in two, enhancing depolymerization, and the protein complex Arp2/3 nucleates branches from existing filaments, creating new plus ends at each branch tip and protecting the bound minus ends of branches from depolymerization. These proteins and their associated processes constitute the dendritic nucleation model [2]. This biological model is supported by experiments that show that severing, capping, and branching are all crucial to cell motility [3–7].

In order to gain insight into how the cell controls its structural dynamics it is imperative to understand *quantitatively* how actin morphology can be controlled by the concentrations of these regulatory proteins. To date, theoretical studies of these kinetic processes have either omitted one or more of these critical processes [8–12] or have been restricted to describing the overall amount of polymerization as a function of time [13]. Other treatments of actin-based motility have focused on the interplay of force generation with motility [14–16], and treat the branched actin network either as an elastic continuum or as a collection of uncoupled filaments. In this Letter, we adopt a complementary approach that not only captures many of the critical features of the dendritic nucleation model but also allows the first theoretical investigation of the morphology of the branched network. We confirm biological and biochemical understanding of the proteins involved by

obtaining quantitative agreement with bulk *in vitro* experiments. We extend the approach to explore the interplay between actin morphology and motility near the leading edge of a crawling cell. The agreement of our theory with electron microscopy images of the leading edge of a crawling cell provides strong evidence that the dendritic nucleation model captures the key players in this important form of cell motility.

We introduce a mean-field rate equation formulation for actin structures that undergo polymerization, depolymerization, capping, branching, and severing. We capture key morphological information by retaining length distributions of filaments with free minus ends and of branches. Our formulation is constructed for polar actin assembly with branching (Arp2/3), severing (cofilin), and capping agents, whose action is described by rate constants. Initially, capping is taken into account by assigning a probability for a filament to be capped; for reversible capping, this renormalizes the polymerization rate. Thus, k_+ is the effective polymerization rate constant. The growth rate at the barbed end of a filament is $k_+\rho_m$, where ρ_m is the free monomer concentration. The depolymerization rate is denoted by k_-. Nucleation and dissociation of filament seeds are described by rate constants k_n and k_d [17], respectively. Nucleation of branches is modeled by the rate constant $k_{arp} = k_{arp}^0 \rho_{\text{Arp2/3}} \rho_m^2$ [12,17], where $\rho_{\text{Arp2/3}}$ is the concentration of Arp2/3. Eventually, Arp2/3 dissociates and branches detach at a rate k_{dr} [18]. Severing occurs at a rate $k_s = k_s^0 \rho_s$, where ρ_s is the severing protein concentration [19]. The nucleotide state of the polymerized actin controls the rates of both branching (preferred at ATP-actin sites [20]) and severing (preferred at ADP-actin sites [21]). We therefore consider conversion of ATP-actin to ADP-actin at a rate k_{pr} [22]. The probability that a monomer at distance L from the barbed end of a filament is an ADP-actin monomer is then given by $p(L) = 1 - \exp(-L/l_c)$ [9], where $l_c = k_+\rho_m/k_{pr}$. We allow branching only on ATP-actin monomers and severing only on ADP-actin monomers in filaments.

Unless specified, $k_+ = 8.7\ \mu M^{-1} s^{-1}$ [23], $k_- = 0.03\ s^{-1}$ (estimates are 10^{-2}–10^{-1} [24] depending on conditions), $k_d = 5 \times 10^{-4}\ s^{-1}$ [17], $k_n = 3 \times 10^{-6}\ \mu M^{-1} s^{-1}$ (fitted; see caption of Fig. 1), $k_{arp}^0 = 4.7 \times 10^{-4}\ \mu M^{-3} s^{-1}$ (fitted and consistent with [12]), $k_{dr} = 0.0018\ s^{-1}$ [11,12], $k_s^0 = 4 \times 10^{-5}\ \mu M^{-1} s^{-1}$ (estimated from [19,25]), and $k_{pr} = 0.002\ s^{-1}$ [26]. To capture the morphology we consider (i) the density of actin filaments of length L (in monomer units) with free minus ends (i.e., minus ends that can depolymerize) $\rho_u(L)$, (ii) the density of branches of length L (which have bound minus ends that cannot depolymerize) $\rho_b(L)$, and (iii) the density of monomers ρ_m. In the mean-field bulk case where all rate constants and densities have no spatial dependence, we have

$$
\begin{aligned}
\dot{\rho}_u(L) = &-k_+ \rho_m(\rho_u(L) - \rho_u(L-1)) \\
&+ k_-(\rho_u(L+1) - \rho_u(L)) + k_{dr}\rho_b(L) \\
&- k_s \sum_{L'=1}^{L-1} p(L')\rho_u(L) + \sum_{L'=L+2}^{\infty} k_s p(L)\rho_b(L') \\
&+ \sum_{L'=L+1}^{\infty} k_s(p(L) + p(L'-L))\rho_u(L'),
\end{aligned}
\tag{1}
$$

$$
\begin{aligned}
\dot{\rho}_b(L) = &-k_+ \rho_m(\rho_b(L) - \rho_b(L-1)) - k_{dr}\rho_b(L) \\
&- k_s \sum_{L'=1}^{L-2} p(L')\rho_b(L) + \sum_{L'=L+1}^{\infty} k_s p(L'-L)\rho_b(L'),
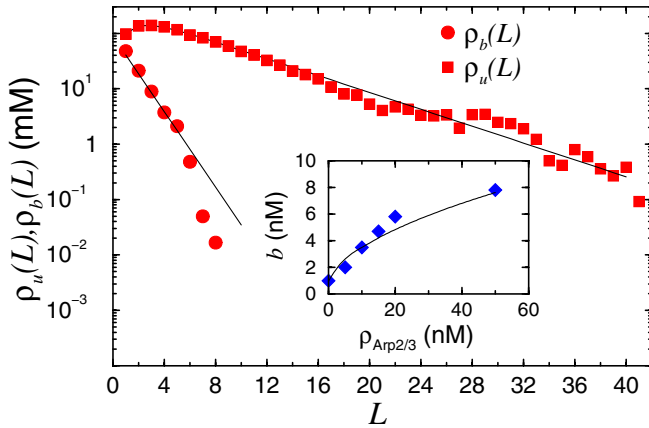\end{aligned}
\tag{2}
$$

FIG. 1 (color online). Length distribution of filaments and of branches (in monomer units), as predicted by our mean-field theory (lines) and as calculated from Brownian dynamics simulations (points), with $k_+ = 15\ \mu M^{-1} s^{-1}$, $k_- = k_{dr} = 100\ s^{-1}$, $k_{arp}/k_+ = 0.015$. Inset: The barbed end concentration as a function of $\rho_{Arp2/3}$, as predicted by mean-field theory (lines) and measured by experiment (points) [28]. Here, k_n and k_{arp}^0 were estimated by fitting to average filament length and branching percentage data from [28] (not shown).

$$
\begin{aligned}
\dot{\rho}_u(2) = &-k_+ \rho_m \rho_u(2) + k_- \rho_u(3) - k_d \rho_u(2) + k_{dr}\rho_b(2) \\
&+ k_n \rho_m^2 + \sum_{L'=4}^{\infty} k_s p(2)\rho_b(L') + \sum_{L'=3}^{\infty} k_s \tilde{p}(L')\rho_u(L'),
\end{aligned}
\tag{3}
$$

$$
\begin{aligned}
\dot{\rho}_b(2) = &-k_+ \rho_m \rho_b(2) - k_{dr}\rho_b(2) \\
&+ k_{arp} \sum_{L=2}^{\infty} \left(\sum_{L'=1}^{L} 1 - p(L') \right)(\rho_u(L) + \rho_b(L)) \\
&+ \sum_{L'=3}^{\infty} k_s p(L'-2)\rho_b(L'),
\end{aligned}
\tag{4}
$$

with $\tilde{p}(L') = p(2) + p(L'-2)$. A fifth equation is the conservation of total number of monomers. These equations are similar to those in Refs. [10–13], though we distinguish between unbranched and branched filaments to quantitatively describe morphology.

We first study the steady state in absence of severing and nucleotide dependence. The length distributions are

$$
\rho_u(L) = Ae^{-L/\lambda_u} + Be^{-L/\lambda_b},
\tag{5}
$$

$$
\rho_b(L) = Ce^{-L/\lambda_b},
\tag{6}
$$

where $\lambda_u = 1/\log(k_-/k_+ \rho_m) \approx k_+ \rho_m/(k_- - k_+ \rho_m)$, $\lambda_b = 1/\log[(k_{dr} + k_+ \rho_m)/k_+ \rho_m] \approx k_+ \rho_m/k_{dr}$. A, B, and C are length independent and depend on the rate constants and total actin concentration. The approximations are valid for $L \gg 1$, which is generally the case *in vivo*, and imply that $k_- \approx k_+ \rho_m$ and $\lambda_b \approx k_-/k_{dr}$.

We performed Brownian dynamics simulations to determine the accuracy of Eqs. (5) and (6) [27]. We have used rates somewhat different from physiological ones to achieve equilibration within reasonable time. Figure 1 shows that the simulations and theory yield length distributions in good agreement with each other with no adjustable parameters at these concentrations. The maximum in $\rho_u(L)$ occurs because branches can fall off and contribute to the pool of unbranched filaments.

We have also compared our calculations to *in vitro* experiments by Blanchoin *et al.* [28]. We neglect severing, depolymerization, and nucleotide-state dependence because those experiments did not contain severing proteins and filaments were stabilized by phalloidin. Our results for the barbed end concentration as a function of Arp2/3 concentration are plotted in the inset of Fig. 1 and are in good agreement with the experiment.

When severing and monomer nucleotide state are included, analytical progress can be best made by using "global" conservation principles at steady state to derive simple, approximate expressions for morphological properties. For example, in steady state, the average total number of branches must be conserved so the rates of destruction and production of branches must balance. The destruction rate is $k_{dr}\sum_{L=2}^{\infty} \rho_b(L)$. The production

rate is $k_{arp}^0 \rho_{\mathrm{Arp2/3}} \rho_m^2 \sum_{L=2}^{\infty} (\sum_{L'=1}^{L} (1-p(L')))(\rho_u(L) + \rho_b(L)) \approx k_{arp}^0 \rho_{\mathrm{Arp2/3}} f(k_-/k_+)^2 \rho_m^{\mathrm{tot}}$, where ρ_m^{tot} is the total actin concentration and f denotes the fraction of polymerized F-actin monomers that are ATP bound and, hence, capable of supporting branching and immune to severing. Equating the two rates yields $\sum_{L=2}^{\infty} \rho_b(L) \approx (k_{arp}^0 \rho_{\mathrm{Arp2/3}}/k_{dr}) f \rho_m^2 (k_-/k_+)^2 \rho_m^{\mathrm{tot}}$.

Similarly, the average number of free filaments is fixed such that $k_s(1-f)\sum_{L=2}^{\infty} L(\rho_u(L) + \rho_b(L)) + k_{dr}\sum_{L=2}^{\infty} \rho_b(L) = k_d \rho_u(2)$. If we assume that $\rho(L)$ can be described by one characteristic length $\bar{L}_u$, implying $\rho_u(2) \approx \rho_m^{\mathrm{tot}}/\bar{L}_u^2$, then $\bar{L}_u = \{k_d/[k_s(1-f) + k_{arp}^0 \rho_{\mathrm{Arp2/3}} f(k_-/k_+)^2]\}^{1/2}$. In steady state, conservation of ATP F-actin implies $f \approx [k_{pr}(\bar{L}_u/k_-) + 1]^{-1}$ such that

$$\bar{L}_u \simeq \left(\frac{k_d(k_{pr}\bar{L}_u + k_-)}{k_s k_{pr}\bar{L}_u + k_{arp}'(\frac{k_-}{k_+})^2 k_-}\right)^{1/2}, \qquad (7)$$

where $k_{arp}' = k_{arp}^0 \rho_{\mathrm{Arp2/3}}$. Comparing the two terms in the denominator, we see that branching does not significantly affect the average length $\bar{L}_u$ until $\rho_{\mathrm{Arp2/3}}$ is at least 4 orders of magnitude larger than ρ_s. *In vitro* motility experiments [3] typically operate in the regime where $\rho_{\mathrm{Arp2/3}} < \rho_s$. So Eq. (7) shows that for large k_s, $\bar{L}_u$ is short and scales as $\bar{L}_u \sim [k_d k_-/(k_s k_{pr})]^{1/3}$. For lower k_s [but $k_s \gg k_{arp}'(k_-/k_+)^2$], $\bar{L}_u$ is larger and shows a more sensitive dependence on k_s: $\bar{L}_u \sim (k_d/k_s)^{1/2}$. The crossover between these two regimes occurs when $\bar{L}_u \sim 10$. On the other hand, when severing is negligible and k_{pr} is small such that sidebranching dominates, then $\bar{L}_u \propto 1/\sqrt{k_{arp}'}$. For small k_s and large phosphate release rates k_{pr}, where endbranching dominates, $\bar{L}_u \propto 1/k_{arp}'$. These scaling predictions are observed in simulations of Eqs. (1)–(4) and are experimentally testable.

Although branching and severing have antagonistic functions, with one process nucleating filaments and the other destroying them, the dependence on nucleotide state allows them to act in concert [13]. To explore this synergy, we examine the density of branches (number of branches per F-actin monomer), another globally conserved quantity in steady state. As k_{pr} increases, branching occurs only near barbed ends, so the branch density will depend on the number density of filaments, which is sensitive to severing. Specifically, $\sum \rho_b \propto \sqrt{k_s} k_{arp}'$. On the other hand, if there is no dependence on nucleotide state, the branch density depends on the total F-actin density, which depends only weakly on k_s. Figure 2(a) is a contour plot of the branch density as a function of ρ_s and $\rho_{\mathrm{Arp2/3}}$. If severing were irrelevant, the contour lines would be horizontal. Figure 2(a) shows that small changes in ρ_s can affect branch density significantly, pointing to cooperativity between branching and severing.

These results suggest that the dependence of branch density on the nucleotide state of monomers in filaments allows the cell to control *multiple* aspects of the morphol-
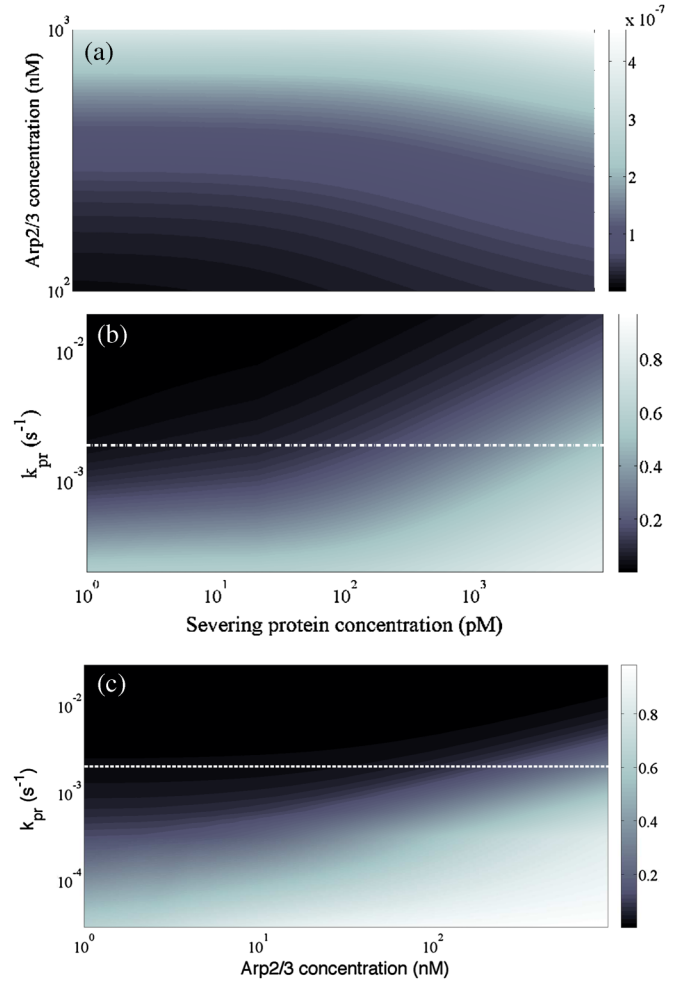

FIG. 2 (color online). (a) Branch density as a function of ρ_s and $\rho_{\mathrm{Arp2/3}}$. Steady-state value of f as a function of k_{pr} and (b) ρ_s with $\rho_{\mathrm{Arp2/3}} = 100$ nM and (c) $\rho_{\mathrm{Arp2/3}}$ with $\rho_s = 10$ pM. In (b) and (c), white dashed lines indicate the *in vivo* value of k_{pr}.

ogy by varying the concentration of severing protein. Figure 2(b) shows the fraction of the ATP-bound monomers in a filament as a function of ρ_s and the phosphate release rate k_{pr}. For small k_{pr}, $f \approx 1$ at all ρ_s, so that branching can occur anywhere on the filament. For large k_{pr}, $f \approx 0$ at all ρ_s so that branching can occur only at barbed ends. For the *in vivo* value $k_{pr} \approx 0.002$ s^{-1}, however, the system crosses over from $f \approx 0$ to $f \approx 1$ over the indicated range of ρ_s, corresponding to the *in vivo* range of filament lengths (roughly 10–500 monomers). Similarly, Fig. 2(c) shows that near the physiological k_{pr} value, the system crosses over from $f \approx 0$ to $f \approx 1$ over the indicated range of Arp2/3 concentration. Thus, Figs. 2(b) and 2(c) suggest that the system is optimized to have a morphology that is maximally responsive to changes of ρ_s, $\rho_{\mathrm{Arp2/3}}$, and k_{pr} under physiological conditions.

We now consider the coupling of morphology to motility by confining the system between two hard walls both moving with velocity v. The "front" wall models the leading edge of the cell while the "back" wall denotes
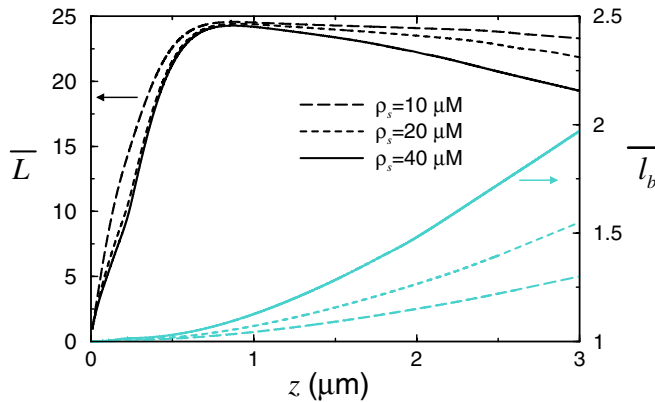
PHYSICAL REVIEW LETTERS

FIG. 3 (color online). Dark lines: $\bar{L}$ versus distance from leading edge z for different cofilin concentrations ρ_s. Here, $v = 0.1 \, \mu\text{m}/\min$, $v_t = 25 \, \mu\text{m/s}$, $D = 5 \, \mu\text{m}^2/\text{s}$, $z_{arp} = 0.1 \, \mu\text{m}$, $z_s = 2 \, \mu\text{m}$, $k_c = 1 \, \text{s}^{-1}$, $k_{uc} = 0.01 \, \text{s}^{-1}$ with 1 μM Arp2/3 and 100 μM actin (at the upper end of the physiological range). Light lines: Distance between branches versus distance for the same parameters.

the back edge of the lamellipodium. Because capping is necessary to motility [7], we extend Eqs. (1)–(4) to explicitly include a capping rate k_c and uncapping rate k_{uc} by defining four populations of filaments: capped and uncapped branched and unbranched filaments. Now $\rho_u(L, t, z)$ denotes the density of capped or uncapped filaments of length L whose barbed ends are at distance z from the front wall. Details of this calculation are described in Ref. [29]. Briefly, we assume exponentially decaying concentration profiles for Arp2/3 and G-actin away from the leading edge, with decay lengths z_{arp} [30] and D/v_t, respectively, where D is the G-actin diffusion constant and v_t is the transport velocity of monomers towards the surface [31]. We assume an inverted exponential with rise length z_s for severing protein to model the nucleotide dependence of severing. Finally, we assume that filaments are at an angle of $\theta = 35°$ with respect to the leading edge [32].

In steady state, we find that branching, severing, and capping are all needed to obtain a morphology that is consistent with experiments. Branching in the front is needed to help the system "keep up" with the wall by nucleating new filaments. Capping towards the front channels new filament growth into shorter branches and thus increases filament density. Finally, severing is needed to replenish the free monomer supply. Figure 3 shows the steady-state morphology for the system with a moving surface. We plot the average filament length $\bar{L}$ and the average distance between branches (left and right axes, respectively) as functions of distance z from the front wall. The average filament length is short near the surface, and increases to approximately 100 nm at a distance of roughly 0.5 μm from the surface before decreasing towards zero at the back of the lamellipodium. We find $\bar{L}$ decreases with increasing severing protein concentration

ρ_s, as expected. The average branch distance increases monotonically with z; the higher ρ_s is the greater is the increase in the branch distance with z. In short, Fig. 3 implies short branched filaments within the first micron of the leading edge, with longer, less branchy filaments further away. These observations are consistent with electron microscopy images of the lamellipodium in crawling keratocytes [33], suggesting that the dendritic nucleation model indeed captures the minimal set of proteins involved in the absence of cross-linkers. For tens of micromolar concentrations of severing protein, the lamellipodium length (the distance the lamellipodium extends into the cell from the leading edge) is tens of microns, reasonably consistent with experimental observations [33]. The predicted length increases with actin concentration.

[1] H. Lodish *et al.*, *Molecular Cell Biology* (W. H. Freeman, New York, 1995), 3rd ed.
[2] T. D. Pollard *et al.*, Annu. Rev. Biophys. Biomol. Struct. **29**, 545 (2000).
[3] D. Pantaloni *et al.*, Science **292**, 1502 (2001).
[4] A. Y. Chan *et al.*, J. Cell Biol. **148**, 531 (2000).
[5] M. Bailly *et al.*, Curr. Biol. **11**, 620 (2001).
[6] H. Aizawa *et al.*, J. Cell Biol. **132**, 335 (1996).
[7] T. Loisel *et al.*, Nature (London) **401**, 613 (1999).
[8] A. Mogilner and L. Edelstein-Keshet, Biophys. J. **83**, 1237 (2002).
[9] L. Edelstein-Keshet and G. Bard Ermentrout, J. Math. Biol. **43**, 325 (2001).
[10] A. E. Carlsson, Phys. Rev. Lett. **92**, 238102 (2004).
[11] A. E. Carlsson, Biophys. J. **89**, 130 (2005).
[12] A. E. Carlsson *et al.*, Biophys. J. **86**, 1074 (2004).
[13] A. E. Carlsson, Biophys. J. **90**, 413 (2006).
[14] K. Kruse *et al.*, Phys. Biol. **3**, 130 (2006).
[15] A. Mogilner and G. Oster, Biophys. J. **84**, 1591 (2003).
[16] A. T. Dawes *et al.*, J. Theor. Biol. **242**, 265 (2006).
[17] D. Pantaloni *et al.*, Nat. Cell Biol. **2**, 385 (2000).
[18] A. M. Weaver *et al.*, Curr. Biol. **11**, 370 (2001).
[19] K. Moriyama and I. Yahara, EMBO J. **18**, 6752 (1999).
[20] I. Ichetovkin *et al.*, Curr. Biol. **12**, 79 (2002).
[21] T. D. Pollard and G. G. Borisy, Cell **112**, 453 (2003).
[22] D. Vavylonis *et al.*, Proc. Natl. Acad. Sci. U.S.A. **102**, 8543 (2005).
[23] H. N. Higgs *et al.*, Biochemistry **38**, 15 212 (1999).
[24] J. R. Kuhn and T. D. Pollard, Biophys. J. **88**, 1387 (2005).
[25] J. Du and C. Frieden, Biochemistry **37**, 13 276 (1998).
[26] R. Melki *et al.*, Biochemistry **35**, 12 038 (1996).
[27] K.-C. Lee and Andrea J. Liu (unpublished).
[28] L. Blanchoin *et al.*, Nature (London) **404**, 1007 (2000).
[29] A. Gopinathan *et al.* (unpublished).
[30] M. Bailly *et al.*, J. Cell Biol. **145**, 331 (1999).
[31] D. Zicha *et al.*, Science **300**, 142 (2003).
[32] I. Maly and G. Borisy, Proc. Natl. Acad. Sci. U.S.A. **98**, 11 324 (2001).
[33] T. Svitkina *et al.*, J. Cell Biol. **145**, 1009 (1999).